ACS OMEGA

http://pubs.acs.org/journal/acsodf

Article

Study of Gallium-Doped Zinc Oxide Thin Films Processed by Atomic Layer Deposition and RF Magnetron Sputtering for Transparent Antenna Applications

Petru Lunca-Popa,* Jean-Baptiste Chemin, Noureddine Adjeroud, Veronika Kovacova, Sebastjan Glinsek, Nathalie Valle, Mohamed El Hachemi, Stéphanie Girod, Olivier Bouton, and Jérôme Polesel Maris

Cite This: *ACS Omega* 2023, 8, 5475−5485

Read Online

ACCESS | Metrics & More | Article Recommendations | Supporting Information

ABSTRACT: Gallium-doped zinc oxide (GZO) films were fabricated using RF magnetron sputtering and atomic layer deposition (ALD). The latter ones demonstrate higher electrical conductivities (up to 2700 S cm^{-1}) and enhanced charge mobilities (18 cm^2 V^{-1} s^{-1}). The morphological analysis reveals differences mostly due to the very different nature of the deposition processes. The film deposited via ALD shows an increased transmittance in the visible range and a very small one in the infrared range that leads to a figure of merit of 0.009 Ω^{-1} (10 times higher than for the films deposited via sputtering). A benchmarking is made with an RF sputtered indium-doped tin oxide (ITO) film used conventionally in the industry. Another comparison between ZnO, Al:ZnO (AZO), and Ga:ZnO (GZO) films fabricated by ALD is presented, and the evolution of physical properties with doping is evidenced. Finally, we processed GZO thin films on a glass substrate into patterned transparent patch antennas to demonstrate an application case of short-range communication by means of the Bluetooth Low Energy (BLE) protocol. The GZO transparent antennas' performances are compared to a reference ITO antenna on a glass substrate and a conventional copper antenna on FR4 PCB. The results highlight the possibility to use the transparent GZO antenna for reliable short-range communication and the achievability of an antenna entirely processed by ALD.

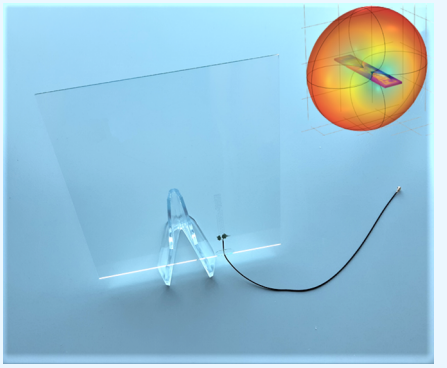

INTRODUCTION

Transparent conducting oxides (TCOs) constitute a class of materials simultaneously showing high electric conductivities and an optical transparency in the visible range, two antagonistic properties. They are used in a wide range of applications including low-emissivity windows, optoelectronic devices, transparent contacts for solar cells, touch screens, flat panel displays, architectural smart glasses, and electromagnetic shielding devices.[1] Although, lately, the p-type TCOs have started to be developed and thoroughly studied,[2−4] the market is dominated by the n-type materials. The most widely used now is the indium tin oxide with electrical conductivities and visible transparency beyond 3000 S/cm and 90%, respectively. However, with indium world reserve seriously diminishing[5,6] and the expanding need for transparent optoelectronic devices, the development of alternative TCOs represents a crucial problem to be solved. This requires the use of more earth-abundant materials with a low environmental impact. Among the multitude of n-type oxides, the zinc oxide (ZnO) based materials[7] are seen as a relatively inexpensive and earth-abundant viable alternative. In the intrinsic form, ZnO is way too resistive for TCO applications, and donor dopants are required for surpassing this. Aluminum (abundant) or gallium (with a supply potential 10 times higher than indium[8]) are the most widespread materials used in this case. Aluminum (AZO)- and gallium (GZO)-doped zinc oxides are the most promising alternatives to ITO, demonstrating electric conductivities up to 1200 S cm^{-1} and visible transparencies of around 90%.[9−11] GZO has started to be preferred lately because of stability issues encountered in the case of AZO, a result of the differences among the ionic radius (Ga^{3+}: 0.47 Å; Al^{3+}: 0.39 Å; and Zn^{2+}: 0.60 Å) as well as the high probability of inactive Al_2O_3 phase formation.[9,12] ZnO-based materials are deposited using basically all known synthesis methods, as many of its applications require polycrystalline films. A special approach is required if a high degree of crystalline quality or purity is envisaged as in the case of advanced optoelectronic

Received: October 18, 2022
Accepted: January 11, 2023
Published: January 30, 2023

https://doi.org/10.1021/acsomega.2c06574
ACS Omega 2023, 8, 5475−5485

Table 1. Literature Survey over the Performances of Transparent Antennas Made of TCOs for BLE/WiFi Communication at around 2.45 GHz

materials[a]	thickness[b] (nm)	Rs (Ω/□))	process	T_{max}[c] (°C)	size[d] (cm)	gain (dBi)	S11[e] (dB)	Transmittance[f] (%)	IoT demo[g]	ref
GZO	1400	2.4	PE-MBE	710	47 × 2.5	2.1	−14	75	no	34
sapphire					60 × 10					
AZO	400	53	ALD	-	14 × 6	−0.4	-	-	yes	35
glass					33 × 26	−3.6				
AZO	109	2100	PVD	450	190 × 32	4.9	−26	-	no	36
Si wafer					190 × 130					
AZO	600	-	FEA modeling	-	36 × 23	6.4	−16	-	no	37
quartz					60 × 50					
FTO	1100	7	spray pyro	480	diam. 15.6	0.05	−16	-	no	38
Pyrex										
ITO	460	10.4	PVD	-	26 × 25	-	−30	74	no	39
glass					26 × 25					
GZO	200	18	ALD	250	41 × 5	-	−2	83	yes	*
glass					150 × 150					
GZO	200	206	PVD	250	41 × 5	-	−2	84	yes	*
glass					150 × 150					
ITO	200	32	PVD	250	41 × 5	-	−2.5	84	yes	*
glass					150 × 150					

[a]Antenna and substrate. Underlines in the case where a ground plane on a bottom layer was used. [b]Thickness of the thin film. [c]Maximum temperature of the antenna fabrication process. [d]Antenna and substrate lateral dimensions. [e]Reflection coefficient. [f]Transparency in visible range. [g]Demonstration of use for IoT communication (Bluetooth); *: this work; -: values not mentioned in the reports.

devices.[7] Molecular beam epitaxy[13] (MBE) or pulsed laser deposition[14] (PLD) is used because they are able to ensure a high degree of control of deposition conditions. From the technological point of view, RF magnetron sputtering and ALD thin film processing are the most adequate because they are already at a "manufacturing-at-scale" level. These methods have their own advantages and disadvantages,[15] but both are well implemented at the technological scale. On the one hand, the sputtering deposition (a physical vapor deposition (PVD) technique) is well mastered as it has been used from more than 50 years at an industrial level. It ensures high deposition rates and a good film−substrate adherence. However, the ballistic nature (high kinetic energies of the particles involved) leads to substantial difficulties in controlling particle/surface processes and an increase of the defect's density.[16] On the other hand, the ALD (a chemical vapor deposition (CVD) method) ensures a high level of growth control and allows uniform and conformal depositions on substrates with complex geometries (as a non-line-of-sight method).[17] Unlike PVD that uses tipically solid targets, the ALD processing uses organometallic precursors in the gas phase, allowing a fine tuning of the stoichiometry and an excellent reproducibility on it along the whole growth process.

The properties of zinc oxide based thin films strongly depend on their surface morphology and crystallographic structures. Consequently, processing efforts are required for them to fit specific applications. For instance, the nonpolar m-plane (100) and a-plane (110) of ZnO crystals are beneficial for high-efficiency LED and transparent conductive oxide applications,[18,19] whereas polar c-plane (002) ZnO thin films are employed for potential applications containing sensors,[20] nanogenerators,[21] piezotronics,[22] and energy harvesters[23] because of the spontaneous and piezoelectric polarization effects along the *c* axis. Doping ZnO improves the electrical conductivity and opens avenues as an ITO challenger for new applications for transparent electronics. However, to fully harvest the possibilities offered by ZnO-based materials, mastering the deposition process is a must, and in consequence, a lot of research is concentrated in understanding the AZO and GZO deposition process. For example, in the case of PVD synthesis, the scientific community has lately been focusing on the detrimental role of the oxygen ions on the uniformity of deposited films.[11,24,25] In the case of ALD synthesis, the latest efforts are oriented toward the understanding of the influence of the dopant/Zn ratio on the growth mode and optoelectronic properties.[26]

In the context of 5G deployment as the backbone of trillions of Internet of Things (IoT) devices, innovative designs of antennas represent a major challenge in terms of efficiency in small volume but also as an object that must integrate into their environment in a harmonious way.[27,28] Various designs of embedded antennas exist for every type of network such as WiFi, Bluetooth MESH, LP-WAN, NB-IoT, LoRa, SigFox, ISM 791-960 MHz, or cellular. Choosing the adequate antenna design for an IoT wireless connectivity depends on the type of link devices, and therefore, antenna technology depends on the application in question. The most popular WiFi/WLAN, Bluetooth, and ZigBee connectivity might be the first choice for access points.[29] For our project goals, we used a commercial patch antenna design, Siretta Echo 17.[30] This is a coplanar patch antenna that shows a promising design by its efficiency, bandwidth, radiation pattern, gain, and miniaturized dimensions (by its meandered structure[31−33]) and, most importantly, does not require a back side ground plane, simplifying its fabrication process.

These characteristics make it easier for the optimization and impedance tuning and straightforward deposition process onto glass substrates. Moreover, making the IoT relay antennas invisible by means of transparent electronics thus represents another promising prospect for the telecommunication markets.[40−42] The frequencies proposed for the upcoming 5G network would result in shorter broadcast distances and network dead zones. Additional access points and signal repeaters embedded into the existing infrastructure help

https://doi.org/10.1021/acsomega.2c06574
ACS Omega 2023, 8, 5475−5485

mitigate these issues through embedding transparent antennas into the windows by means of metallic meshes[43,44]/nanowires[45] or transparent conductive oxides (TCOs).[28,35,46] The present article demonstrates the first TCO-based transparent antenna processed entirely by ALD. Optically transparent antennas based on both AZO[47] and GZO[48] have been previously demonstrated (comprehensive reviews on TCO-based antennas here[28,49,50]). AZO antennas were fabricated to operate at 11 and 45 GHz, and a GZO antenna was fabricated to operate at 2.4 GHz. The GZO material demonstrated higher optical transparency with equivalent conductivity as ITO against film thickness.[51] Table 1 summarizes the reported performances of the transparent antennas on glass set for 2.4 GHz, a frequency suitable for IoT communication by Bluetooth, WiFi, and ZigBee. It is interesting to notice that there are not a lot of works on it, and there is only one work demonstrating a real IoT communication (AZO antenna) as shown in this paper. The first part of the present work is focused on the comparison of optoelectronic properties of ZnO, AZO, and of GZO films fabricated by ALD. All films were synthesized in-house, and the processes were optimized for maximum transparency and conductivity for 15 × 15 cm glass substrates as well for matching the impedance requirements. The GZO films demonstrate superior properties with electric conductivities and figure of merit twofold than those of AZO. We then fabricated GZO films by ALD and RF sputtering with the aim to find an optimum fabrication path. Structural, morphological, chemical, and optoelectronic properties are compared. The films fabricated via the ALD process present a figure of merit 10 times higher than those synthesized using sputtering, with higher carrier mobilities and densities. The GZO films demonstrate very good infrared reflection properties, being transparent only for visible wavelengths. In the last part, an application case of GZO thin films for transparent patch antennas is proposed by means of subtractive lithography processing and integration in a short-range BLE communication setup. The monitoring of the emission/reception signal is done against the distance, and comparisons with a conventional ITO material transparent (also in-house synthesized and optimized) antenna and a commercial copper track FR4 PCB patch antenna are made. When comparing with current state of the art in the field, our work is the only one demonstrating high optical transmittance in the visible light with a low sheet resistance value for GZO ALD with a real case demonstration of IoT Bluetooth communication until a range of more than 10 m. Furthermore, we can notice our low temperature processing at 250 °C to get such a low sheet resistance compared to the best ones: GZO but by PE-MBE at 710 °C process temperature and FTO but by spray pyrolysis at 480 °C process temperature.

EXPERIMENTAL DETAILS

Thin Film Deposition. All TCO films were deposited on 15 × 15 cm, 2 mm thick glass substrates.

Atomic Layer Deposition. Thin film depositions were performed on a Beneq TFS500 ALD system equipped with a deposition chamber for 300 mm diameter wafers. The substrate was placed in the reactor of the ALD, which was heated by thermal resistors placed in the chamber to control its temperature (T_{ch}). The temperature of the reactor was measured close to the substrate by a thermocouple to be representative of the sample temperature. For all samples investigated in the present work, the chamber temperature was kept at 250 °C. During the deposition, the reactor pressure was about 3−5 mbar. Diethylzinc (DEZ, $(C_2H_5)_2Zn$), trimethylaluminum (TMA, $Al_2(CH_3)_6$), and trimethylgallium (TMG, $Ga(CH_3)_3$) (Strem Chemicals, Inc., France) were used as metal precursors, whereas water was used as the second precursor for oxygen. The ALD deposition cycles consisted of four steps of different time lengths: metal precursor (t_1), first purge (t_{1p}), water precursor (t_2), and second purge (t_{2p}). During the purge steps, only the argon carrier gas was flowing continuously to remove the precursor leftovers that did not react on the surface and the secondary products of reaction. The structures of ALD cycles were as follows: for ZnO deposition: t_1 = 150 ms/t_{1p} = 20 s/t_2 = 200 ms/t_{2p} = 10 s; for Al_2O_3 deposition: t_1 = 200 ms/t_{1p} = 20 s/t_2 = 100 ms/t_{2p} = 20 s; and for Ga_2O_3 deposition: t_1 = 50 ms/t_{1p} = 20 s/t_2 = 100 ms/t_{2p} = 10 s. In the case of Al:ZnO, the deposition sequence was 30 layers of ZnO followed by 1 layer of Al_2O_3. In the case of Ga:ZnO (GZO), the deposition sequence was 20 layers of ZnO followed by 1 layer of Ga oxide, as we observed that these stack configurations lead to the maximum conductivity. The following parameters were optimized for the maximum figure of merit matching impedance conditions in an antenna: injection times (metallic precursor and water), reactor temperature, and the content of dopant within the ZnO. Here, we use the term "Ga oxide" for the ALD deposition of Ga and water, although there are reports mentioning that H_2O does not react efficiently with the TMG terminated surface at low temperatures.[52] It is thus very probable that the layers demonstrate a serious deficiency in oxygen atoms. Furthermore, each sequence was repeated until the targeted thickness was acquired. For example, repeating the GZO sequence 23 times led to a film thickness of about 50 nm. The thickness of the ZnO after 480 loops was about 80 nm. All films were ended by depositing 20 loops of ZnO (≈3.3 nm) as a capping layer.

Physical Vapor Deposition. The indium oxide/tin oxide target had a 90/10 wt % composition (99.99% pure from Kurt J. Lesker). The deposition conditions were as follows: substrate rotation of 5 rpm, room temperature, 98 ppm of argon, 2 ppm of O_2, pressure of 6 × 10^{-3} mbar, and 100 W of power for plasma generation. A thickness of 100 nm was reached after a deposition of 11 min. A 20 min atmospheric post annealing step at 300 °C was used to improve the optical properties and conductivity of ITO. For the GZO films, the pressure was maintained at 5 × 10^{-3} mbar by using an argon flow of 50 sccm. Prior to the deposition, the substrate was heated at 350 °C. A 2 in. diameter target with a purity of 99.95% and a composition of ZnO/Ga_2O_3 95/5 wt % was used. The power of the RF power supply was 100 W, corresponding to a power density of 4.9 W/cm^2. The substrate was placed at a distance of 12 cm from the target, and a 30° angle between the target and the substrate was maintained during the deposition. The angular speed of the substrate was also set at 5 rpm. Again, the processes were previously optimized for maximum figure of merit.

XRD Characterization. The phase structure was investigated using a Bruker D8 Discover diffractometer with Cu Kα radiation of 0.154 nm operating at 40 kV and 40 mA in parallel beam configuration. The substrates used in this case were Si (001) wafers. The locked coupled theta-2 theta method was used for this study.

Elemental and Chemical Composition. The elemental and chemical composition of the samples was investigated by

https://doi.org/10.1021/acsomega.2c06574
ACS Omega 2023, 8, 5475−5485

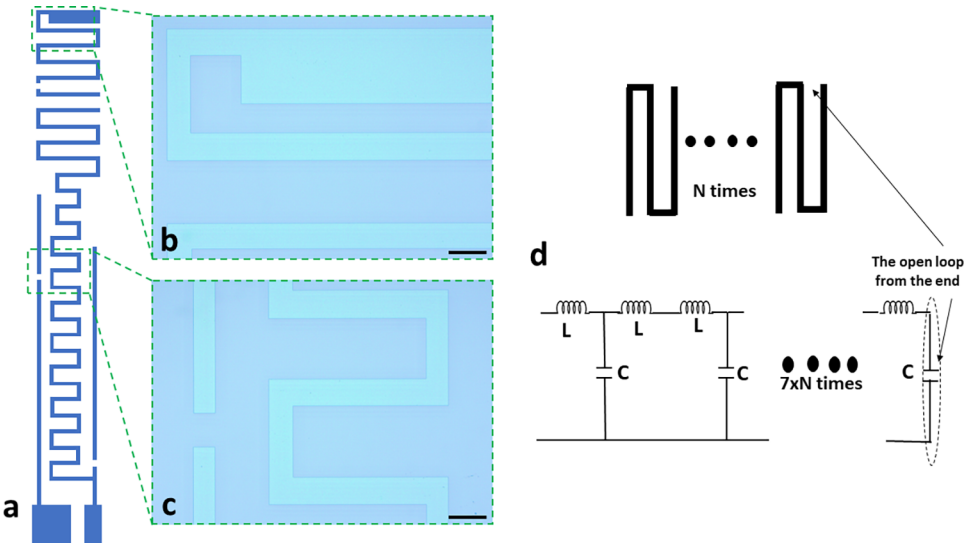

Figure 1. (a) Design of the patch antenna. (b and c) Optical micrographs of the lithographed and wet etched tracks (GZO) on a glass slide (scale bar = 500 um). (d) Approximative lumped model of the antenna.

X-ray photoelectron spectroscopy (XPS) on a Kratos Axis Ultra DLD system equipped with a monochromatic Al Kα X-ray source (hν = 1486.7 eV) operating at 225 W. The etching was carried out with an Ar^+ ion beam operating at 2 kV and 100 μA oriented at 45°. High-resolution spectra were acquired at the surface after 600, 1200, 1800, and 2400 s.

Secondary Ion Mass Spectroscopy (SC-Ultra). The following analytical conditions were ensured during the sampling of the films deposited on silicon substrates: primary ions: Cs^+ bombardment; impact energy: 1 keV; primary beam intensity: 4 nA; scanned area: 250 × 250 μm^2; secondary: positive ions; analyzed area size: 63 μm in diameter; MCs_x^+ mode (M: element of interest, x = 1 or 2); and low mass resolution (400).

Electrical Properties. Electrical measurements were performed using an ECOPIA van der Pauw−Hall effect measurement system (HMS 3000 from Microworld) equipped with a magnet generating a magnetic field of 1.5 T. A second check measurement for sheet resistance was performed using conventional four probes in linear configuration with a Keithley 2614B source meter still at room temperature, with similar results.

Scanning Electron Microscopy (SEM). Thin films deposited on Si substrates were inspected using an FEI Helios 50 high-resolution system. Through-lens-detector (TLD) in secondary electron mode imaging was engaged.

Optical Properties (of Films Deposited on Glass). They have been measured on a Perkin Elmer Lambda 1050 spectrophotometer equipped with 150 mm integrating spheres and Si (UV−vis) and InGaAs (NIR) detectors. Transmittance and reflectance spectra were acquired for films deposited on glass substrates in the range from 2500 to 250 nm.

Lithography Patterning of Transparent Antennas. To process patch antennas for benchmarking performances, we patterned the same antenna's shape by lithography on ITO made by PVD, GZO by PVD, and GZO by ALD deposited on glass slides (2 mm thickness, 150 × 150 mm^2) as illustrated on Figure 1a−c. We used the design of the Echo 17 commercial antenna from Sirreta.[30] This model is specifically tuned to provide optimal performance for the 2.4−2.5 GHz frequency band. It consists of a meander line-type antenna, well documented over the literature.[31−33] Within this model, every linear segment of the antenna can be modeled by an LC circuit (lumped model) as illustrated on Figure 1d. After a thorough cleaning of the glass slides coated with the TCO thin films with acetone, isopropanol, and DI water; drying; and dehydration on a hot plate (120 °C, 15 min), the patterning was performed by a preliminary deposition of an S1813 photoresist (MicroChemicals) followed by laser lithography processing (MLA150, Heidelberg Instruments Mikrotechnik) of the antenna electrodes.

The pattern of the antenna was revealed in MF-319 Developer (MicroChemicals), rinsed with DI water, and postbaked at 115 °C for 2 min on a hot plate. The wet etching to manufacture ITO tracks was realized inside a solution mixing HCl 6 M and $FeCl_3{\cdot}6H_2O$ 0.2 M for 25 min at room temperature. The wet etching to manufacture GZO tracks was realized inside a solution of Al etchant (Alfa Aesar, reference 44581.WY). After the etching, the samples were plunged inside a DI water beaker to stop the reaction and dried. Finally, the remaining S1813 photoresist was removed with acetone, and the glass slides with TCO tracks were cleaned in DI water, dried, and heated at 130 ° C for 10 min on a hot plate.

Design of the Antenna. We based the design of the conductive tracks for the TCO transparent patch antennas on a standard reference one for WiFi/WLAN communication with a frequency tuning between 2.4 and 2.5 GHz (Siretta Echo 17 WiFi/WLAN PCB Antenna). This antenna can be used with WiFi, Bluetooth, Zigbee, and ISM 2450 based applications. The reference antenna is based on an FR4 PCB of 0.8 mm thickness with copper tracks of 18 μm thickness. We used it during the communication testing for benchmarking the transmission/reception performances compared to the TCO transparent antennas we realized in this work.

RF Measurements. The reflection coefficient S_{11} parameter of the TCO antennas was measured using NanoVNA V2 (NanoRFE) Vector Network Analyzer (VNA). The antennas were fitted with 10 cm long coaxial cables with UF.L connectors chosen to be connected to the Bluetooth Low Energy (BLE) module described in the next section. A UF.L to SubMiniature version A (SMA) adapter was used to connect

https://doi.org/10.1021/acsomega.2c06574
ACS Omega 2023, 8, 5475−5485

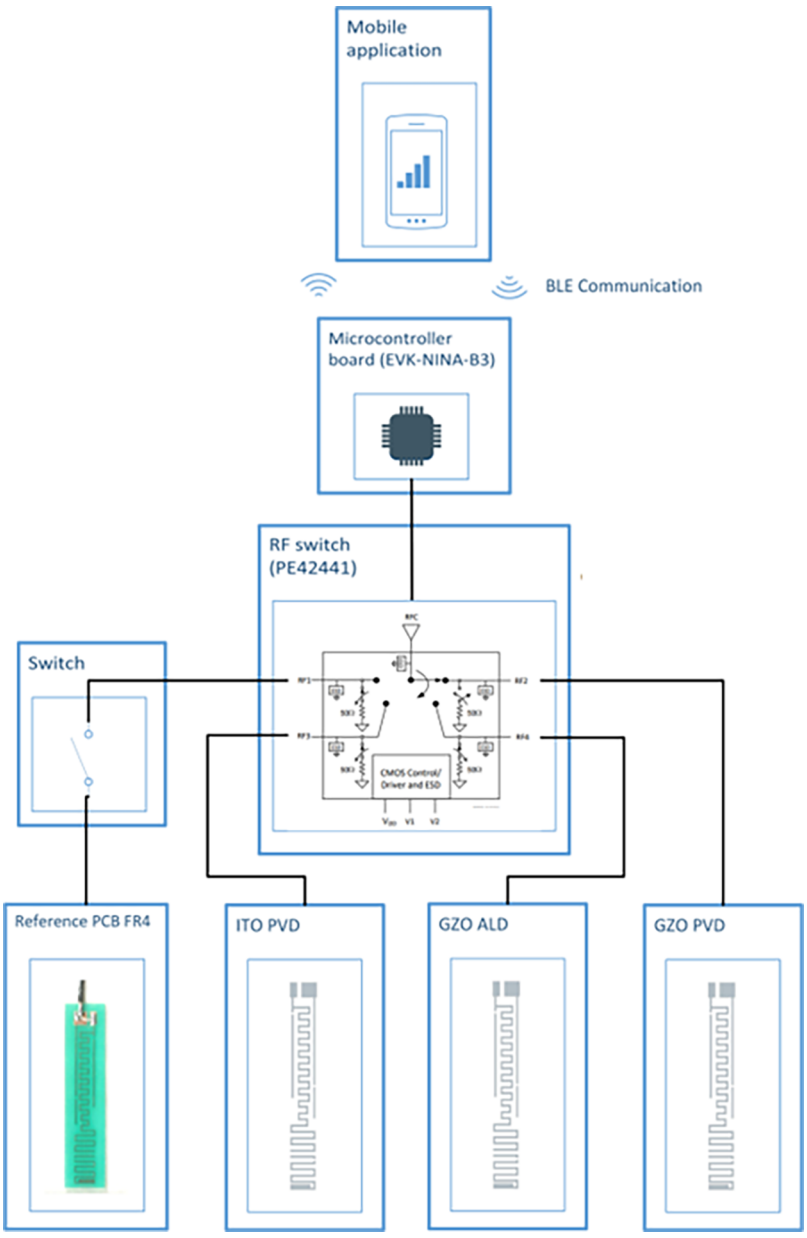

Figure 2. Schematic of the setup for measuring the RSSI of the antennas.

the antenna to the VNA. The two pins of the coaxial cable were fixed on the patch antenna electrodes with conductive silver loaded epoxy glue (reference: 186-3616, RS) cured at room temperature for 24 h. Before measuring the antennas' RF response, a full one-port calibration with an open, a short, and a matched 50 Ω load standard was performed. To avoid problems with electromagnetic reflections at the end of the antenna cables, it was essential to use cables of the same length for each of the calibration standards as for the antennas under test. The S_{11} reflection coefficient was measured with an output power from the VNA of 1 mW, i.e., 0 dBm, in the frequency range from 1.5 to 3.5 GHz with a total of 150 points equally spaced in frequency for data acquisition. Measurements were also performed on the reference antenna of copper tracks on the FR4 PCB.

Testing of the Antennas. To compare the communication performances of the three patch antennas (ITO PVD, GZO PVD, and GZO ALD and the reference copper electrodes on FR4 PCB), we integrated them on a Bluetooth Low Energy (BLE) 5.0 communication setup (Figure 2). A four-port/one-input/output RF switch (PE42441, pSEMI, matched at 50 Ω) was used to connect the four patch antennas by UF.L to SMA adapters, with one port remaining not connected by a switch in a second stage of measurement to get a reference communication signal without an antenna (Figure 2). The RF switch works in both ways of transmission and reception with the antennas. The input/output connector of the RF switch was connected to the SMA antenna connector of a card equipped with a microcontroller and a BLE module (EVK-NINA-B3, NINA-B301 chipset, u-blox AG, matched at 50 Ω). A BLE beacon application to send battery status was coded by the ARDUINO IDE[53] and flashed onto the microcontroller card. The same periodic signal of this BLE beacon was sent sequentially through each patch antenna by each port of the RF switch with a periodic switching command signal of 4 s from the microcontroller. A Samsung Galaxy A40

https://doi.org/10.1021/acsomega.2c06574
ACS Omega 2023, 8, 5475−5485

Table 2. Summary of Optoelectronic Properties of 50 nm Thick ZnO, Al:ZnO, and Ga:ZnO Thin Films Deposited by ALD in This Work

	σ (S cm^{-1})	n (cm^{-3})	mobility (cm^2 V^{-1} s^{-1})	R_{Sheet} ($\Omega/\square$)	T (400−800 nm)	FOM (kΩ^{-1})
ZnO	113	4.4×10^{19}	16	1763	0.78	0.05
AZO	752	6.20×10^{20}	7.5	266	0.82	0.5
GZO	1408	9.3×10^{20}	9.4	142	0.85	1

smartphone with the application BLE Analyser (Keuwlsoft, Google Playstore) was used to monitor the RSSI (received signal strength indicator) to compare the efficiency of communication of each patch antenna at a fixed distance between the BLE beacon and the smartphone.

EXPERIMENTAL RESULTS AND DISCUSSIONS

Comparing ZnO, Al:ZnO, and Ga:ZnO Synthesized by Atomic Layer Deposition. To establish the optimum figure of merit (FOM) of thin film materials for transparent antennas, a first study was performed to assess the optoelectronic properties of ZnO, AZO, and GZO. Films with a thickness of 50 nm were deposited on glass and silicon substrates by using ALD. Table 2 depicts a summary of optoelectronic properties of the as-deposited films. The carrier mobility was determined using the Hall effect. The optical transmittance was averaged in the 400−800 nm wavelength interval. The Haake figure of merit (T^{10}/R_{sh}) was calculated in this case.

The zinc oxide nondoped films show a conductivity of 113 S cm^{-1}. This increases to 752 S cm^{-1} when doped with aluminum and to 1408 S cm^{-1} when doped with gallium. The values are generally higher than those reported in the literature (GZO:[10] $n = 4.23 \times 10^{20}$ cm^{-3}, $\sigma = 1282$ S cm^{-1}; AZO:[11,24,26,54] $n = 5.1 \times 10^{20}$ cm^{-3}, $\sigma = 1200$ S cm^{-1}) for similar films deposited by ALD.[55] This important increase is a result of one order of magnitude increase in carrier concentration. The carrier mobility demonstrates a slight decrease in AZO and GZO due to the defects induced by doping in the ZnO matrix. The higher carrier concentration measured in the case of GZO might be the result of using water as oxygen precursor. When ALD is used for fabrication, the AZO and GZO are generally synthesized by intercalating individual layers of Ga or Al oxide between layers of ZnO. However, the TMG[52] precursor is known not to react well with water, and hence, the appearance of a low conductive Ga_2O_3 phase is less probable to occur in the case of the GZO deposition process. This might lead to the direct incorporation of interstitial Ga^{3+} ions into the ZnO and hence the increase of electron concentration. The optical properties of the three films are similar in the visible range (Figure 3) with transmittance of around 80%. The highest is measured for GZO (Table 2) followed closely by AZO and ZnO. However, the situation is different in the infrared region. The optical spectra follow the conductivity trend from ZnO to GZO, a result of the increase of absorption on the free charge carriers. These results demonstrate an increase of the FOM with more than 2 orders of magnitude from nondoped to gallium-doped zinc oxide. Thereby, gallium-doped zinc oxide was chosen to be used as a TCO for integrating within the transparent antenna device described in this work.

Comparing Ga:ZnO Films Synthesized by Atomic Layer Deposition and by RF Sputtering. The second step consisted of comparing GZO films processed by ALD and by PVD. For the sake of completeness, the films were compared with an ITO film deposited by RF sputtering. A reference 100 nm thick film was sputtered, and a summary of optoelectronic properties is shown in Table 3.

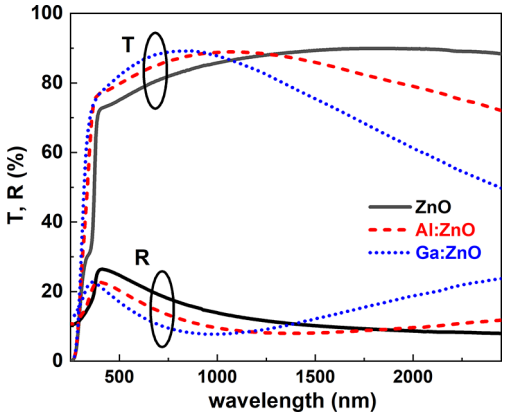

Figure 3. Transmittance (upper lines) and reflection (bottom lines) optical spectra of ZnO (continuous lines), Al:ZnO (dashed lines), and Ga:ZnO (dotted lines) films deposited by ALD. Thickness = 50 nm.

The GZO films fabricated via ALD present figures of merit 10 times higher than those fabricated using PVD. As the optical spectra look similar in the visible range (Figure 4), the improvement of the FOM is a consequence of better electric properties. Moreover, these films present 10 times higher electric conductivity, a result of higher carrier charge concentrations (1 order of magnitude) and higher mobilities (3-folds). The superior properties might be explained by considering the nature of the two processes. In the case of PVD, a composite GZO target was used, and hence, we can consider that the material was transferred from the target to the substrate. The main important parameter here might be considered the substrate temperature with a strong influence on the initial stage of nucleation and growth. The situation is different in the case of ALD. The Ga^{3+} ions are inserted only between the ZnO layers (one loop of trimethyl gallium every 23 loops of diethyl zinc). The process is less energetical (low momentum for the incoming atoms), and hence, the Ga ions will migrate toward thermodynamically stable positions. Moreover, as already mentioned, the use of water as oxygen precursor led to the inhibition of the Ga_2O_3 insulating phase. The ALD deposited films present properties similar with those of the ITO film. The optical behavior is completely different in the IR range. The transmittance decreases with the wavelength as a result of absorption on free carriers. It drops faster for the most conductive films (GZO by ALD and ITO). This behavior is aimed usually in infrared reflecting coatings for windshields and glass windows within the automotive or smart building industries,[56] respectively, as it reflects the solar heat while still being visibly transparent.

Figure 5 shows the top-view and cross-section SEM micrographs for GZO films deposited by ALD and PVD. They look similar, both films showing compacted surfaces. The PVD films (left) seem denser without pores are perpendicular

https://doi.org/10.1021/acsomega.2c06574
ACS Omega 2023, 8, 5475−5485

Table 3. Optoelectronic Properties of GZO (200 nm) Deposited by PVD and by ALD

		σ (S cm^{-1})	n (cm^{-3})	mobility (cm^2 V^{-1} s^{-1})	R_{Sheet} ($\Omega/\square$)	T (400−800 nm)	FOM (kΩ^{-1})
GZO	ALD	2764	1.7×10^{21}	10.4	18	0.83	9
GZO	PVD	242	2.5×10^{20}	6.1	206	0.84	0.8
*ITO**	*PVD*	*3087*	*5.3×10^{20}*	*36.7*	*32*	*0.84*	*5.5*

*The properties of an ITO (100 nm) film RF sputtered are shown for comparison.

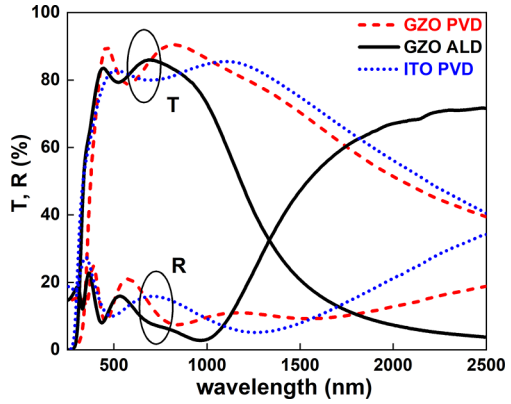

Figure 4. Transmittance and reflection optical spectra for GZO films deposited by ALD (black continuous lines) and PVD (red dashed lines). The spectra of an ITO 100 nm film (blue dotted lines) are shown for reference.

to the surface. This is the result of the highly energetic sputtering process, where incident atoms with high kinetic energy values are impinged toward the substrate. On the contrary, for the film synthesized by ALD, some small voids are visible within the bulk of the films, and a detailed analysis was previously published.[57] This might be confirmed by the XRD locked coupled analysis from Figure 5b. The (004) Si substrate peak (2θ = 69.15° position) is clearly visible on the diffractogram corresponding to the ALD fabricated film. This is a result of the fact that the X-rays succeed in sampling the substrate beyond the GZO film. For the PVD denser films, this substrate peak is much weaker, a result of the higher compactness of the deposited films (the GZO film covers "better" the substrate). In both cases, the films present a high degree of (002) texture around the 2θ = 34.4° position. Other ZnO characteristic diffraction peaks are visible but with very low intensities at the following 2θ positions: 2θ = 31.8° (100), 2θ = 36.2° (101), and 2θ = 47.4° (102). A shift toward smaller 2θ angles is evidenced in the case of the (002) peak, a consequence of replacing the Zn^{2+} with a radius of 0.60 Å with Ga^{3+} having a radius of 0.47 Å. This shift is more pronounced for the PVD synthesized films, a consequence of a greater content of gallium in these films (as explained in the following section).

The SIMS analysis results are presented in Figure 6. They reveal higher Ga and O contents in sputtered films. As already

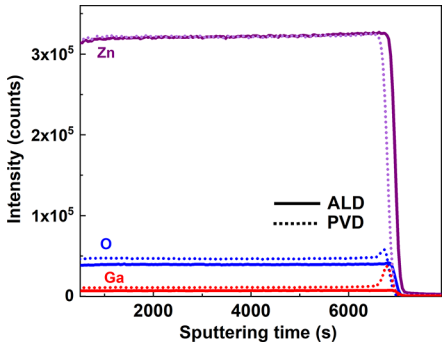

Figure 6. Secondary ion mass spectroscopy analysis on GZO films fabricated by ALD and by PVD.

mentioned, the PVD uses a composite 5% Ga doped ZnO target, and consequently, the composition of the deposited films can follow that of the target. However, in the case of ALD, Zn, Ga, and O are deposited successively (layer by layer). The incoming ions are moving freely until they are chemisorbed by the previous layer forming the compound. This develops self-limiting surface reactions between gaseous precursor molecules and the substrate.

The thermodynamic conditions during ALD processing for Ga doping in ZnO are restrictive; the compound not chemically bonded to the surface might be removed during the purging step. Additionally, Ga and O count intensity overshoots are observed at the interface with silicon in the

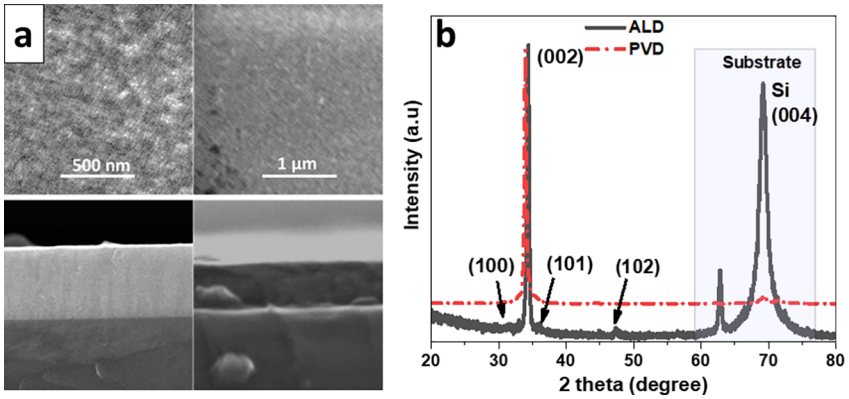

Figure 5. Morphological and crystallinity characterizations of GZO thin films. (a) Top-view and cross-section SEM micrographs of the films deposited by PVD (left) and ALD (right). (b) XRD locked coupled diffractograms for 200 nm thin films.

https://doi.org/10.1021/acsomega.2c06574
ACS Omega 2023, 8, 5475−5485

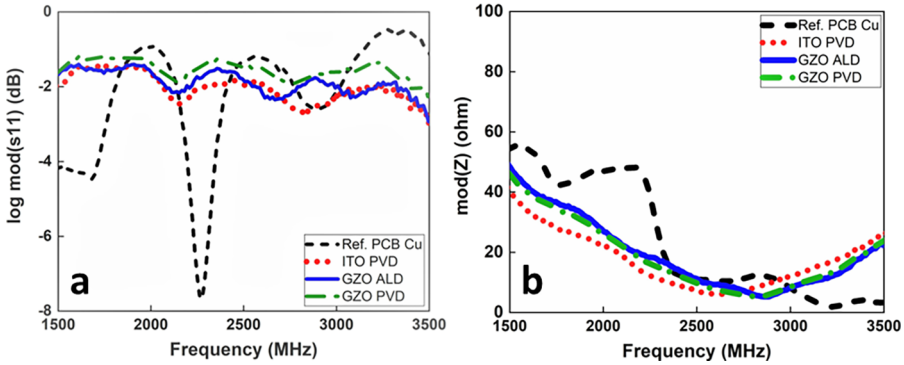

Figure 7. VNA measurements for the four patch antennas (ITO PVD, GZO PVD, GZO ALD, ref. PCB Cu = copper electrodes/FR4 PCB). (a) Reflection coefficient parameter S_{11}. (b) Z_{11} impedance modulus.

sample for the PVD films. We can presume then that on the Si substrate, the formation of gallium oxide such as Ga_2O_3 is favored by PVD compared with Ga:ZnO. This is not the case for ALD films where the deposition of Ga starts on previously deposited ZnO layers. Finally, a higher Zn/O ratio is observed in ALD films. Considering the similar Zn content for the two films, this difference might be a result of a lower O content. This is expected because of the already reported low reactivity between water (as precursor for oxygen) and TMG (Ga precursor).[52] This also might explain the higher free carrier concentration as the low oxygen content might impede the formation of a parasitic less conductive Ga_2O_3 phase. Hence, it is probable that in the case of the ALD, there are more available Ga^{3+} ions for doping the ZnO. However, the Ga intensity measured seems to be too high to consider it as a dopant concentration. In other words, one might ask if gallium might still be considered as a dopant considering its content level. Dopants are conventionally added in small concentrations (<1000 ppm). They may be interstitials or substitute into the crystal structure. They do not normally result in the formation of a new phase as would be the case for alloying agents resulting in the formation of new phases. However, this debate is out of the scope of this paper addressing the most suited TCO thin film processing for the proposed antenna device. Within this framework, we claim that the GZO films deposited by ALD are the most suitable for incorporating within the transparent device. They present the highest figure of merit with a conductivity beyond 2700 S cm^{-1} and a transparency above 85% in the visible range.

Performances of GZO Thin Films for Transparent Antennas. The design of the patch antenna is shown in Figure 1a. Its total length and width are 41.5 and 5.4 mm, respectively. The width of the transparent conductive tracks is 360 μm. The same geometry was used for all antennas, which were built from different track materials. We can expect that the differences between the antennas' performances are a result of the differences between deposited thin film materials. The dimension scaling effects are expected to be the same for all "geometrically" similar antennas. Optical micrographs of the lithographed and wet etched GZO tracks on a glass slide are shown in Figure 1b and c. The reflection coefficient S_{11}, measured using VNA, is shown in Figure 7a. The reference antenna FR4 PCB Cu has several minima, with the most pronounced one at 2.26 GHz close to the expected 2.4 GHz frequency from the specifications for Bluetooth communication. TCO antennas based on GZO and ITO thin films, on the other hand, show much less pronounced minima. Those of main interest are present at 2.14, 2.13, and 2.15 GHz for GZO by ALD, GZO by PVD, and ITO by PVD antennas, respectively. The impedance Z_{11} modulus (Figure 7b) shows non monotonous frequency dependence in all three cases. Its values for each previously spotted S_{11} minima are 20.8, 20.5, 16, and 41 Ω for the GZO by ALD, GZO by PVD, ITO by PVD, and FR4 PCB Cu antennas, respectively.

The setup in indoor conditions for measurements of the antennas performances is based on the Bluetooth Low Energy 5.0 (BLE) communication setup with a four-ports/one-input/output RF switch (Figure 2) connecting sequentially the four patch antennas. Three of them are based on the TCOs described in this article: GZO by ALD, GZO by PVD, and ITO by PVD. The fourth one is the reference FR4 PCB copper patch antenna. The configuration is set to acquire sequential transmission measurements of each antenna from the beacon signal (microcontroller card) to a distanced smartphone by using the application BLE Analyser (Keuwlsoft, Google Playstore) as shown in Figure S1 (Supporting Information). The received signal strength indicator (RSSI) (Figure 8) of the

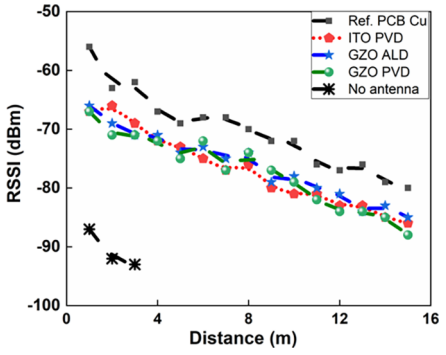

Figure 8. Distance monitoring of the RSSI for each patch antenna, also considering the case of the nonconnected antenna on the RF switch.

antennas was measured as a function of distance between the antenna and receiver.[58] With increasing distance from 1 to 15 m, the RSSI value of TCO antennas decreased from −66 to −86 dBm, respectively. Compared to the reference FR4 PCB Cu antenna, these values are lower by a difference between 8 and 5 dBm for the whole distance.

Considering the RF measurements by VNA, thin film TCO antennas compared to the reference thick copper FR4 PCB demonstrated lower reflection coefficient parameter S_{11} values

https://doi.org/10.1021/acsomega.2c06574
ACS Omega 2023, 8, 5475−5485

with a shift of the minima toward lower frequency.[59] Numerical modeling of the ITO antennas with submicrometric track thicknesses, below the skin depth, is in accordance with the experimental measurements by VNA with less pronounced resonance minima and a shift of this one to lower frequency due to an increase of the electrical resistivity (Figure S2 Supporting Information). The simultaneous measurements of the impedance modulus Z_{11} of TCO antennas highlight a substantial mismatch between the Z_{11} impedance value of around 20 Ω for the corresponding S_{11} minima compared to the expected standardized value of 50 Ω for optimized RF power transfer in waveguides. The reference thick copper FR4 PCB antenna with an impedance value of 41 Ω is more in accordance with the 50 Ω matching expected. Considering that we transferred an existing patch antenna design for TCO antennas but optimized only for a copper-based antenna on FR4 PCB, we could expect that the change of the substrate by glass (with a dielectric constant of 5 to 6 compared to a lower dielectric constant of 3.8 to 4.8 for FR4 PCB) and the antenna track material by either GZO or ITO induced a dramatic shift of the performances in the RF regime. The RSSI monitoring against distance between each antenna connected to the same BLE beacon and a smartphone demonstrated similar performances of the TCO antennas for GZO (by both ALD and PVD) and ITO but lower performance compared to the copper-based antenna on FR4 PCB. Here also, the impedance mismatch between the TCO antennas and the BLE beacon module (adapted to 50 Ω) could explain a substantial part of lost transmission power.[60] An additional study, not in the frame of this work, would be the design optimization by modeling of the ITO and GZO patch antennas to meet the 50 Ω matching around 2.4 GHz. Nevertheless, even if not optimized for impedance matching, the GZO antennas demonstrated reliable BLE connection in transmission and reception until a distance of about 10 m between the beacon and the smartphone with a minimum RSSI of −80 dBm. That performance level is good enough for many daily-life IoT applications to connect smart devices where the use of a transparent antenna makes sense for miniaturization and invisibility of the electronics for aesthetic goals (e.g., smart responsive glass windows, mirrors, eyeglasses, watches).

CONCLUSIONS

In this work, we demonstrate Ga:ZnO (GZO) as an efficient TCO alternative for substituting the ITO within transparent antennas. When fabricated by ALD, this material presents better optoelectronic properties when compared with ZnO and Al:ZnO, a consequence of a better incorporation of Ga^{3+} within the ZnO structure and the lack of parasitic Ga_2O_3 phase. The GZO films fabricated by ALD show higher electric conductivities (2700 S cm^{-1}) and carrier mobilities (18 cm^2 V^{-1} s^{-1}) when compared with films synthesized by sputtering. The differences might be explained by considering that the sputtering PVD is a process far from equilibrium, in contrast with the ALD that is a process occurring closer to the thermodynamic equilibrium. We thus illustrate the first transparent antenna processed entirely by using the ALD. This method allows high-quality coatings and opens the possibility to use substrates with complicated out-of-plane geometries for instance to integrate transparent antennas in complex 3D shapes of IoT connected devices. Finally, we demonstrate that GZO by ALD based transparent antennas have comparable radiofrequency properties for IoT short-range communication with those using the consecrated indium-doped tin oxide as TCO. This work might play an important role in proposing a scalable TCO process for industrial manufacturing of transparent parts for RF systems within the actual challenge of searching for alternatives to replace the indium element for transparent electronics and "invisible" devices for IoT.

ASSOCIATED CONTENT

Supporting Information

The Supporting Information is available free of charge at https://pubs.acs.org/doi/10.1021/acsomega.2c06574.

More details about monitoring RSSI and antenna radiation pattern modeling using COMSOL (PDF)

AUTHOR INFORMATION

Corresponding Author

Petru Lunca-Popa − *Materials Research and Technology Department (MRT), Luxembourg Institute of Science and Technology (LIST), L-4422 Belvaux, Luxembourg;* orcid.org/0000-0003-4278-7668; Email: petru.luncapopa@list.lu

Authors

Jean-Baptiste Chemin − *Materials Research and Technology Department (MRT), Luxembourg Institute of Science and Technology (LIST), L-4422 Belvaux, Luxembourg;* orcid.org/0000-0002-3749-787X

Noureddine Adjeroud − *Materials Research and Technology Department (MRT), Luxembourg Institute of Science and Technology (LIST), L-4422 Belvaux, Luxembourg*

Veronika Kovacova − *Materials Research and Technology Department (MRT), Luxembourg Institute of Science and Technology (LIST), L-4422 Belvaux, Luxembourg*

Sebastjan Glinsek − *Materials Research and Technology Department (MRT), Luxembourg Institute of Science and Technology (LIST), L-4422 Belvaux, Luxembourg;* orcid.org/0000-0002-5614-0825

Nathalie Valle − *Materials Research and Technology Department (MRT), Luxembourg Institute of Science and Technology (LIST), L-4422 Belvaux, Luxembourg*

Mohamed El Hachemi − *Materials Research and Technology Department (MRT), Luxembourg Institute of Science and Technology (LIST), L-4422 Belvaux, Luxembourg*

Stéphanie Girod − *Materials Research and Technology Department (MRT), Luxembourg Institute of Science and Technology (LIST), L-4422 Belvaux, Luxembourg*

Olivier Bouton − *Materials Research and Technology Department (MRT), Luxembourg Institute of Science and Technology (LIST), L-4422 Belvaux, Luxembourg*

Jérôme Polesel Maris − *Materials Research and Technology Department (MRT), Luxembourg Institute of Science and Technology (LIST), L-4422 Belvaux, Luxembourg;* orcid.org/0000-0003-0457-619X

Complete contact information is available at: https://pubs.acs.org/10.1021/acsomega.2c06574

Notes

The authors declare no competing financial interest.

The manuscript was written through contributions of all authors. All authors have given approval to the final version of the manuscript.

https://doi.org/10.1021/acsomega.2c06574
ACS Omega 2023, 8, 5475−5485

■ ACKNOWLEDGMENTS

We would like to thank Dr. Torsten Granzow for his relevant advice concerning VNA measurements. We gratefully acknowledge Dr. Damien Lenoble and the financial support provided by the MRT Core Technologies internal funding of LIST.

■ REFERENCES

(1) Minami, T. Transparent Conducting Oxide Semiconductors for Transparent Electrodes. *Semicond. Sci. Technol.* **2005**, *20*, S35−S44.
(2) Moreira, M.; Afonso, J.; Crepelliere, J.; Lenoble, D.; Lunca-Popa, P. A Review on the P-Type Transparent Cu−Cr−O Delafossite Materials. *J. Mater. Sci.* **2022**, *57*, 3114−3142.
(3) Wiebeler, H.; Kormath Madam Raghupathy, R.; Mirhosseini, H.; Kühne, T. D. Virtual Screening of Nitrogen-, Phosphorous- and Halide-Containing Materials as p-Type Transparent Conductors. *J. Phys. Mater.* **2021**, *4*, No. 015004.
(4) Kim, T.; Yoo, B.; Youn, Y.; Lee, M.; Song, A.; Chung, K. B.; Han, S.; Jeong, J. K. Material Design of New P-Type Tin Oxyselenide Semiconductor through Valence Band Engineering and Its Device Application. *ACS Appl. Mater. Interfaces* **2019**, *11*, 40214−40221.
(5) Stevenson, R. *Endangered elements*; Physics World https://physicsworld.com/a/endangered-elements/.Accesed 12.12.2019
(6) Frenzel, M.; Mikolajczak, C.; Reuter, M. A.; Gutzmer, J. Quantifying the Relative Availability of High-Tech by-Product Metals − The Cases of Gallium, Germanium and Indium. *Resour. Policy* **2017**, *52*, 327−335.
(7) Janotti, A.; Van De Walle, C. G. Fundamentals of Zinc Oxide as a Semiconductor. *Rep. Prog. Phys.* **2009**, *72*, 126501.
(8) Rhodes, C. J. *Endangered Elements, Critical Raw Materials and Conflict Minerals*; SAGE Publications: 2019; Vol. *102*. DOI: 10.1177/0036850419884873.
(9) Ellmer, K.; Bikowski, A. Intrinsic and Extrinsic Doping of ZnO and ZnO Alloys. *J. Phys. D: Appl. Phys.* **2016**, *49*, 413002.
(10) Ponja, S. D.; Sathasivam, S.; Parkin, I. P.; Carmalt, C. J. Highly Conductive and Transparent Gallium Doped Zinc Oxide Thin Films via Chemical Vapor Deposition. *Sci. Rep.* **2020**, *10*, 638.
(11) Khan, S.; Stamate, E. Comparative Study of Aluminum-Doped Zinc Oxide, Gallium-Doped Zinc Oxide and Indium-Doped Tin Oxide Thin Films Deposited by Radio Frequency Magnetron Sputtering. *Nanomaterials* **2022**, *12*, 1539.
(12) Dixon, S. C.; Scanlon, D. O.; Carmalt, C. J.; Parkin, I. P. N-Type Doped Transparent Conducting Binary Oxides: An Overview. *J. Mater. Chem. C* **2016**, *4*, 6946−6961.
(13) Li, Q.; Ying, M.; Zhang, M.; Cheng, W.; Li, W.; Liao, B.; Zhang, X. Structural Characterization and Surface Polarity Determination of Polar ZnO Films Prepared by MBE. *Appl. Nanosci.* **2021**, *187*, 1−8.
(14) Ciolan, M. A.; Motrescu, I. Pulsed Laser Ablation: A Facile and Low-Temperature Fabrication of Highly Oriented n-Type Zinc Oxide Thin Films. *Appl. Sci.* **2022**, *12*, 917.
(15) Matthews, A.; Holmberg, K. PVD and CVD Coatings. In *Encyclopedia of Tribology*; Wang, Q. J., Chung, Y.-W., Eds.; Springer US: Boston, MA, 2013; pp. 2705−2711. DOI: 10.1007/978-0-387-92897-5_724.
(16) Chennupatti, J.; Pearton, S. *Zinc Oxide Bulk, Thin Films and Nanostructures*; Chennupati, J., Pearton, S., Eds.; Elsevier Science Ltd, 2006. DOI: 10.1016/B978-0-08-044722-3.X5000-3.
(17) Wack, S.; Lunca Popa, P.; Adjeroud, N.; Vergne, C.; Leturcq, R. Two-Step Approach for Conformal Chemical Vapor-Phase Deposition of Ultra-Thin Conductive Silver Films. *ACS Appl. Mater. Interfaces* **2020**, *12*, 36329−36338.
(18) Liu, Y.; Li, Y.; Zeng, H. ZnO-Based Transparent Conductive Thin Films: Doping, Performance, and Processing. *J. Nanomater.* **2013**, *2013*, 1−9.
(19) Wang, T.; Wu, H.; Zheng, H.; Wang, J. B.; Wang, Z.; Chen, C.; Xu, Y.; Liu, C. Nonpolar Light Emitting Diodes of M-Plane ZnO on c-Plane GaN with the Al_2O_3 Interlayer. *Appl. Phys. Lett.* **2013**, *102*, 1−9.
(20) Loh, K. J.; Chang, D. Zinc Oxide Nanoparticle-Polymeric Thin Films for Dynamic Strain Sensing. *J. Mater. Sci.* **2011**, *46*, 228−237.
(21) Briscoe, J.; Dunn, S. Piezoelectric Nanogenerators - a Review of Nanostructured Piezoelectric Energy Harvesters. *Nano Energy* **2015**, *14*, 15−29.
(22) Joly, R.; Girod, S.; Adjeroud, N.; Nguyen, T.; Grysan, P.; Klein, S.; Menguelti, K.; Vergne, C.; Polesel-Maris, J. Polymeric Cantilevered Piezotronic Strain Microsensors Processed by Atomic Layer Deposition. *Sens. Actuators, A* **2020**, *315*, 112280.
(23) Wang, P.; Du, H. ZnO Thin Film Piezoelectric MEMS Vibration Energy Harvesters with Two Piezoelectric Elements for Higher Output Performance. *Rev. Sci. Instrum.* **2015**, *86*, No. 075002.
(24) Norrman, K.; Norby, P.; Stamate, E. Preferential Zinc Sputtering during the Growth of Aluminum Doped Zinc Oxide Thin Films by Radio Frequency Magnetron Sputtering. *J. Mater. Chem. C* **2022**, *10*, 14444−14452.
(25) Stamate, E. Spatially Resolved Optoelectronic Properties of Aldoped Zinc Oxide Thin Films Deposited by Radiofrequency Magnetron Plasma Sputtering without Substrate Heating. *Nanomaterials* **2019**, *10*, 1−11.
(26) Swatowska, B.; Powroźnik, W.; Czternastek, H.; Lewińska, G.; Stapiński, T.; Pietruszka, R.; Witkowski, B. S.; Godlewski, M. Application Properties of ZnO and AZO Thin Films Obtained by the ALD Method. *Energies* **2021**, *14*, 6271.
(27) Duixian, L.; Zhang, Y. *Antenna-in-Package Technology and Applications*; John Wiley and Sons, 2020.
(28) Green, R. B.; Guzman, M.; Izyumskaya, N.; Ullah, B.; Hia, S.; Pitchford, J.; Timsina, R.; Avrutin, V.; Ozgur, U.; Morkoc, H.; Dhar, N.; Topsakal, E. Optically Transparent Antennas and Filters: A Smart City Concept to Alleviate Infrastructure and Network Capacity Challenges. *IEEE Antenn. Propag. Mag.* **2019**, *61*, 37−47.
(29) *Selecting an Antenna for Your IoT Project*; Antenova Ltd. https://embeddedcomputing.com/application/networking-5g/5g/antenna-selection-for-iot-projects . Accesed 12.12.2022
(30) *Siretta. Enabling Industrial IoT*; Siretta https://www.siretta.com/products/antennas/echo-17/ . Accesed 12.12.2022
(31) Ripin, N.; Sulaiman, A. A.; Rashid, N. E. A. An Equivalent Circuit Model of Miniature Double E-Shaped Meander Line Printed Monopole Antenna. *J. Telecommun. Electron. Comput. Eng.* **2018**, *10*, 59−63.
(32) Das, A.; Dhar, S.; Gupta, B. Lumped Circuit Model Analysis of Meander Line Antennas. *Mediterr. Microw. Symp.* **2011**, 21−24.
(33) Chen, J. H.; Yang, C. K.; Cheng, C. Y.; Yu, C. C.; Hsu, C. H. Gain Enhancement of a Compact 2.4-GHz Meander Antenna Using Inductive Feed and Capacitive Load. *Microw. Opt. Technol. Lett.* **2017**, *59*, 2598−2604.
(34) Green, R. B.; Toporkov, M.; Ullah, M. D. B.; Avrutin, V.; Ozgur, U.; Morkoc, H.; Topsakal, E. An Alternative Material for Transparent Antennas for Commercial and Medical Applications. *Microw. Opt. Technol. Lett.* **2017**, *59*, 773−777.
(35) Jaakkola, K.; Tappura, K. Exploitation of Transparent Conductive Oxides in the Implementation of a Window-Integrated Wireless Sensor Node. *IEEE Sens. J.* **2018**, *18*, 7193−7202.
(36) Zamudio, M. E.; Busani, T.; Tawk, Y.; Costantine, J.; Christodoulou, C. Design of AZO Film for Optically Transparent Antennas. In *2016 IEEE International Symposium on Antennas and Propagation (APSURSI)*; IEEE Sensors Council 2016; pp. 127−128. DOI: 10.1109/APS.2016.7695772.
(37) Awalludin, M.; Ali, M. T.; Mamat, M. H. Transparent Antenna Using Aluminum Doped Zinc Oxide for Wireless Application. *ISCAIE 2015−2015 IEEE Symp. Comput. Appl. Ind. Electron.*; IEEE 2015, *2* (10), 33−36. DOI: 10.1109/ISCAIE.2015.7298323.
(38) Sheikh, S.; Shokooh-Saremi, M.; Bagheri-Mohagheghi, M. M. Transparent Microstrip Patch Antenna Based on Fluorine-Doped Tin Oxide Deposited by Spray Pyrolysis Technique. *IEEE Microwaves, Antenn. Propag.* **2015**, *9*, 1221−1229.
(39) Raad, H.; White, C.; Schmitzer, H.; Tierney, D.; Issac, A.; Hammoodi, A. A 2.45 GHz Transparent Antenna for Wearable Smart Glasses. *Prog. Electromagn. Res. Symp.* **2017**, *2017*, 99−102.

https://doi.org/10.1021/acsomega.2c06574
ACS Omega 2023, 8, 5475−5485

(40) Yazdani, R.; Yousefi, M.; Aliakbarian, H.; Oraizi, H.; Vandenbosch, G. A. E. Miniaturized Triple-Band Highly Transparent Antenna. *IEEE Trans. Antennas Propag.* **2020**, *68*, 712−718.
(41) Lee, S.; Choo, M.; Jung, S.; Hong, W. Optically Transparent Nano-Patterned Antennas: A Review and Future Directions. *Appl. Sci.* **2018**, *8*, 901.
(42) Hong, W.; Lim, S.; Ko, S.; Kim, Y. G. Optically Invisible Antenna Integrated Within an OLED Touch Display Panel for IoT Applications. *IEEE Trans. Antennas Propag.* **2017**, *65*, 3750−3755.
(43) Kang, S. H.; Jung, C. W. Transparent Patch Antenna Using Metal Mesh. *IEEE Trans. Antennas Propag.* **2018**, *66*, 2095−2100.
(44) Yu, S.; Lee, S.; Lee, H.; Park, Y. B. Study of Mesh Pattern for Optically Transparent Flexible Antenna with Feedline. *Appl. Sci.* **2021**, *11*, 10002.
(45) Goliya, Y.; Rivadeneyra, A.; Salmeron, J. F.; Albrecht, A.; Mock, J.; Haider, M.; Russer, J.; Cruz, B.; Eschlwech, P.; Biebl, E.; Becherer, M.; Bobinger, M. R. Next Generation Antennas Based on Screen-Printed and Transparent Silver Nanowire Films. *Adv. Opt. Mater.* **2019**, *7*, 1900995.
(46) Mohd Ali, N. I.; Misran, N.; Mansor, M. F.; Jamlos, M. F. Transparent Solar Antenna of 28 GHz Using Transparent Conductive Oxides (TCO) Thin Film. *J. Phys. Conf. Ser.* **2017**, *852*, No. 012036.
(47) Zamudio, M. E.; Behzadirad, M.; Christodoulou, C.; Busani, T. Optimization of AZO Films for Integrating Optically Transparent Antennas with Photovoltaics. *Appl. Phys. Lett.* **2017**, *110*, 234101.
(48) Lozovski, V. Z.; Lienau, C.; Tarasov, G. G.; Vasyliev, T. A.; Zhuchenko, Z. Y. Configurational Resonances in Absorption of Metal Nanoparticles Seeded onto a Semiconductor Surface. *Results Phys.* **2019**, *12*, 1197−1201.
(49) Alobaidi, O. R.; Chelvanathan, P.; Tiong, S. K.; Bais, B.; Uzzaman, M. A.; Amin, N. Transparent Antenna for Green Communication Feature: A Systematic Review on Taxonomy Analysis, Open Challenges, Motivations, Future Directions and Recommendations. *IEEE Access* **2022**, *10*, 12286−12321.
(50) Sayem, A. S. M.; Lalbackhsh, A.; Esselle, K. P.; Buckley, J. L.; O'Flynn, B.; Simorangkir, R. B. V. B. Flexible Transparent Antennas: Advancements, Challenges, and Prospects. *IEEE Open J. Antenn. Propag.* **2022**, *3*, 1109−1133.
(51) Park, S. M.; Ikegami, T.; Ebihara, K. Effects of Substrate Temperature on the Properties of Ga-Doped ZnO by Pulsed Laser Deposition. *Thin Solid Films* **2006**, *513*, 90−94.
(52) Comstock, D. J.; Elam, J. W. Atomic Layer Deposition of Ga_2O_3 Films Using Trimethylgallium and Ozone. *Chem. Mater.* **2012**, *24*, 4011−4018.
(53) *ARDUINO IDE software*; Smart Projects https://www.arduino.cc/en/software . Accesed 12.12.2022
(54) Luka, G.; Krajewski, T. A.; Witkowski, B. S.; Wisz, G.; Virt, I. S.; Guziewicz, E.; Godlewski, M. Aluminum-Doped Zinc Oxide Films Grown by Atomic Layer Deposition for Transparent Electrode Applications. *J. Mater. Sci.: Mater. Electron.* **2011**, *22*, 1810−1815.
(55) www.atomiclimits.com. https://www.atomiclimits.com/alddatabase/. Accesed 12.12.2022
(56) Butt, M. A.; Fomchenkov, S. A.; Kazanskiy, N. L.; Ullah, A.; Ali, R. Z.; Habib, M. Infrared Reflective Coatings for Building and Automobile Glass Windows for Heat Protection. *Opt. Technol. Telecommun.* **2017**, *10342*, 103420.
(57) Nguyen, T.; Adjeroud, N.; Guennou, M.; Guillot, J.; Fleming, Y.; Papon, A. M.; Arl, D.; Menguelti, K.; Joly, R.; Gambacorti, N.; Polesel-Maris, J. Controlling Electrical and Optical Properties of Zinc Oxide Thin Films Grown by Thermal Atomic Layer Deposition with Oxygen Gas. *Results Mater.* **2020**, *6*, 100088.
(58) Rodas, J.; Fernández, T. M.; Iglesia, D. I.; Escudero, C. J. Multiple Antennas Bluetooth System for RSSI Stabilization. *Proc. 4th IEEE Internatilonal Symp. Wirel. Commun. Syst. 2007*, ISWCS 2007, 652−656. DOI: 10.1109/ISWCS.2007.4392421.
(59) Esmaeilkhah, A.; Ghobadi, C.; Nourinia, J.; Majidzadeh, M. On Effect of Planar Scaling on Microstrip Patch Antenna Performance. *Adv. Electromagn.* **2018**, *8*, 23−29.
(60) Li, R. L.; Pan, B.; Laskar, J.; Tentzeris, M. M. A Novel Low-Profile Broadband Dual-Frequency Planar Antenna for Wireless Handsets. *IEEE Trans. Antennas Propag.* **2008**, *56*, 1155−1162.

https://doi.org/10.1021/acsomega.2c06574
ACS Omega 2023, 8, 5475−5485